Modeling the effect of middle ear canal area variation

Jont B. Allen
Dept. of Computer and Electrical Engineering
The Beckman Inst. Urbana IL

April 30, 2015

Abstract

Modeling the ear canal and tympanic membrane (TM) has key implications for clinical practice. However this modeling has proven to be difficult, due to the complex nature of wave propagation on and around the TM, and due to the variable area and shape of the ear canal. This report is focused on the impact of middle canal area changes on wave propagation. Here it is shown by example how canal area variations introduce an allpass filtering effect (i.e., dispersive wave propagation). A secondary goal is to explain how area variations may be approximated as a wave-digital filter, as implemented in Parent and Allen (2010) (PA-10). This model was not described analytically, rather was defined as a circuit. Here the basic assumptions of the digital wave guide approach are justified and equations for the PA-10 circuit are derived. It is proved that the ME model is lossless, passive, stable and dispersive.

Introduction

Modeling the properties of the middle ear has many important applications, including diagnostics of the middle and inner ear, speech perception, binaural hearing, and auditory processing of our environment. The ear canal impedance $Z_c(s)$ is one of the most important noninvasive middle ear diagnostic measures and is needed for characterizing and modeling clinical middle ear measurements. It is required for many applications. The canal impedance may be accurately defined up to at least 20 [kHz] (Moller, 1960; Rabinowitz, 1981; Lynch et al., 1982; Allen, 1986; Voss and Allen, 1994). Above that frequency the concept of acoustic impedance is confounded by the presence of higher order modes (HOM), namely non-planer wave propagation. This cutoff frequency (f_c) is determined by the cross-sectional geometry of the ear canal. In humans the ear canal is about 2.5 [cm] long, and the average area is about 0.442 [cm^2] (the average diameter is 7.5 [mm]), with a canal characteristic impedance $z_0 = \rho c/A$ of ≈93.21 [CGS acoustic ohms].

The ear canal is a classical wave-guide. Wave-guides are defined as having axial, but not radial, wave propagation. Wave guides are frequently nonuniform in cross-sectional area. Such is the case of the ear canal. An interesting and important question is: *"How does a variable canal area modify the input impedance of the ear canal?"* While this question has been directly addressed (Farmer-Fedor and Rabbitt, 2002), it has not been fully answered. Here we show that in the case of lossless wave propagation, the effect of the variable area is to introduce a frequency dependent (i.e., *allpass*) group delay between the entrance to the canal and the tympanic membrane (TM).

Next we address the question: *"Why (and where) is the ear canal wave planer?"* This question arises due to the complex motion of the TM. There must be some principle that explains why the complex motion of the TM is not coupled to the canal plane wave. This question is closely related

to the first question, regarding the changing area of the canal. It is only because the canal wave is planer that we can even define the canal impedance, so these questions are important to quantitatively understand.

The answers to these two questions go back to the classic wave-guide model. When the wavelength λ is much larger than the cross-sectional dimensions of the wave-guide a (i.e., when $ka < 1$), radial waves cannot propagate, because the wave equation, in the radial direction, is well approximated by Laplace's equation (Rayleigh, 1896, Vol. II, p. 145). In the absence of delay, the wave equation degenerates into Laplace's equation. As discussed below, waves that satisfy Laplace's equation (in the radial and angular directions) become axial plane waves. In the long-wavelength limit, the medium (i.e., air) appears incompressible in the radial direction. This condition is also known as the *quasi-statics (QS) approximation*.

The relation that determines the QS approximation is $\lambda f = c_0$ (c_0 is the speed of sound). The QS constraint is typically stated as $ka < 1$, where a is a *characteristic dimension* (e.g., the radius) and $k = 2\pi/\lambda = \omega/c_0$ is the axial *wave number*. The simple characterization of the wave number, as the reciprocal of the wave length, fundamentally breaks down when the canal area changes, because in this more general cases, the wave number must be *complex-analytic* in the Laplace frequency $s = \sigma + i\omega$. We define the *complex-analytic wave number* as

$$\kappa(s, x) = \alpha(s, x) + jk(s, x). \tag{1}$$

Like an impedance $Z(s)$, $\kappa(s, x)$ is *complex analytic* in s. Complex analytic functions of s result from the Laplace Transform of a *causal* time domain function.

We shall maintain the important distinction that functions of ω are Fourier transforms, whereas causal functions (operators), such as an impedance or wave number, are analytic in s. We typically describe such analytic functions in terms of their poles and zeros. When specifying an analytic function one needs to specify its *region of convergence* (ROC). For causal functions, the ROC is the entire *right half s plane* (RHP).

Once the wave number is known, the pressure may be determined. In terms of $\kappa(s, x)$, waves propagate as (i.e., Eq. C.4)

$$P^+(x, s) \approx P^+(0, s)e^{-\int_0^x [\kappa(x,s)+\frac{1}{2}\partial_x \ln A(x)]dx}. \tag{2}$$

When propagation losses are included, the real part of κ describes the decay of the pressure wave with distance, while its imaginary part characterizes the delay, which must depend on frequency when the canal area varies. This relationship holds even when there are no losses in which case the real part describes the radiated energy.

Characterizing $\kappa(x, s)$ in terms of the reciprocal of a real wavelength fails, since it makes little sense to think of a wavelength having an imaginary part. When κ is independent of x, these factors simplify to $e^{\mp\kappa(s)x}$ and the wave number remains complex due to the losses. For the loss-less case, $\kappa(s) = i\omega/c_0 = i2\pi/\lambda$, and the wave reduces to a simple plane wave $e^{\mp ikx}$.

A condition equivalent to $ka < 1$, which avoids the problem of λ becoming imaginary, may be stated in terms of a *critical frequency* f_c, defined as

$$\omega_c(x) \equiv 2\pi f_c < c_0/a(x). \tag{3}$$

Here c_0 is the speed of sound and $a(x)$ is a characteristic dimension of the canal, such as its radius.[1] For frequencies below ω_c, radial waves are well approximated by Laplace's equation, as discussed below. The speed of sound depends on frequency when losses in the medium are included, however it is always less than the lossless speed c_0.

[1] These two inequalities are equivalent only when λ is real, since complex numbers do not have ordered.

Since the QS approximation depends on the cutoff frequency f_c, above $\omega_c = 2\pi f_c$ the wavelength is less than a ($ka > 1$), resulting in non-planer waves, as described by HOMs (i.e., the medium is not incompressible in the radial direction).

Transmission line modeling methods A proper treatment of guided waves requires the *Webster horn equation* (Webster, 1914) which implicitly assumes a quasi-static (QS) approximation in the radial and angular directions. These are well understood methods, going back more than 100 years (J.W.S. Rayleigh, *The theory of sound*, 1894).

Campbell's 1904 band-limited lumped-parameter wave-filter (Campbell, 1922) is a alternative to the Webster horn equation, based on a band-limited QS approximation of the axial delay. Modern middle ear and cochlear models, based on electrical circuit theory (Wegel and Lane, 1924; Zwislocki, 1950), follow naturally from Campbell's wave-filters.

Modern digital signal processing (DSP) methods (Hamming, 1977), on the other hand, explicitly depend on the unit delay (i.e., thus violating the QS approximation). This has lead to the concept of a digital wave-guide, which is essential when modeling the middle ear, due to the inherent delay in both the ear canal and TM (Puria and Allen, 1998). Thus ME models essentially violate Campbell's axial QS approximation, since axial delays, as represented by the Webster's Horn formulation, are precisely the basis of such digital wave-guide models.

Horn Equation The best known and widely used wave-guide equation is the *Webster Horn Equation* (WHEN) (Webster, 1919; Salmon, 1946a,b)

$$\frac{1}{A(x)}\frac{\partial}{\partial x}A(x)\frac{\partial p(x,t)}{\partial x} = \frac{1}{c_0^2}\frac{\partial^2 p(x,t)}{\partial t^2} \leftrightarrow \frac{s^2}{c_0^2}P(x,\omega). \tag{4}$$

Here $A(x)$ is the area of the wave-guide (i.e., ear canal), $p(x,t) \leftrightarrow P(x,\omega)$ is the pressure in time (left) and frequency, and $\leftrightarrow$ indicates the Laplace transform.

The WHEN is known to be exact in cases where the wave equation separates,[2] such as the cases of spherical ($A(x) \propto x^2$) and cylindrical ($A(x) \propto x$) coordinates, and of course the trivial case of rectangular coordinates ($A(x) = 1$). The solutions for these three cases are spherical Bessel functions, Bessel functions and plane-waves.

The most interesting cases addressed here are when the area is such that the coordinate system is not separable, such as in the case of Salmon Horns (Salmon, 1946a,b), namely for piece-wise analytic areas ($A(x) \equiv \sum a_k x^k$), which includes the important case of the exponential horn, where $A(x) = A_0 e^{2mx}$. Constant m is known as the *flare parameter*.

Reciprocity Since we are specifically addressing the case of the ear canal terminated in the tympanic membrane (TM), it is useful to consider the reciprocal problem, namely how sound is radiated out of the ear canal, given a complex motion of the TM. Reciprocity is a key property in this case.

Specifically lets consider the point to point link from the entrance to the ear canal, at the tragus, to the output at the stapes, which drives the cochlea. In such cases a volume velocity source at the tragus $U_{ts}(x = 0, \omega)$ will deliver an *isometric force* at the stapes $F_{st}(x = L, \omega)|_{U=0}$, which drives the cochlea. For a reciprocal system, an identical volume velocity source at the stapes $U_{st}(x = L, \omega)$ will deliver the same isometric force (pressure$\times$area) at the tragus $P_{ts}(x = 0, \omega)|_{U=0}$. Understanding the limitations of this reciprocity relation is critical when modeling the middle ear. When higher order modes are present how is reciprocity defined? This specific question is discussed by Rayleigh (1896, Vol. II, p. 146).

[2] Separation of variables is known to apply in 11 cases for the wave equation (Morse, 1948)).

1 Analysis of wave propagation in variable-area tubes

We begin by assuming a complex but constrained motion of the TM. Due to the TM boundary conditions (BC), not all motions are allowed, since the TM is pinned at the tympanic ring (TR) and manubrium (the malleus long process). By a simple generalization of Fourier series, the constrained motion of the TM may be expanded as a two-dimensional orthogonal eigen-mode series $\phi_{nm}(\rho,\theta)$, where integers m, n index the modes. For example for the case of a drum in cylindrical coordinates, the eigenmodes are the Bessel functions $J_n(k\rho)e^{jm\theta}$ (Morse, 1948). While these eigenfunctions do not naturally fit the case of the TM, they are adequate for the purpose of the present discussion.

As stated earlier, the cutoff frequencies $f_{n,m}$ may be approximated as $f_{n,m} = c_{tm}/\lambda_{tm}$. This model assumes that waves propagate on the TM. Here $c_{tm} < c_0$ is the velocity of wave propagation on the TM, and λ_{tm} is the wave length of the TM waves. The case for TM wave propagation has been provided by Puria and Allen (1998), based on the experimental determination of TM delay. In that study it was shown that TM waves travel much slower that air-born sound. The role of the TM is to collect the acoustic energy and convert it into transverse mechanical wave motion. The condition $c_{tm} < c_0$ is necessary to obtain good impedance coupling between the air-born sound plane wave and the TM waves. The principle here is virtually identical that that of a loud-speaker, but running in reverse (Hunt, 1982).

This lowest order mode $\phi_{00} = J_0(\rho a)$ is special as its cutoff frequency is zero, corresponding to the volume velocity of the TM, which therefore directly couples to axial plane wave propagation. The mode with the lowest non-zero cutoff frequency is $\phi_{1,0}$ given by $f_c = 1.84c/\pi d \approx 27$ [kHz], where $d = 2a = 7.5$ [mm] (Morse, 1948).

It is important to consider what happens when the area changes. As long as the QS approximation applies (i.e., $ka < 1$ or equivalently $f < f_c = 27$ [kHz]), the result is dispersive (frequency dependent) delay. We may then replace the full wave equation with Eq. 4, by assuming that the transverse (radial and angular pressure gradient) obeys Laplace's equation (Rayleigh, 1896, Vol. II, p. 145)

$$\frac{1}{A(x)}\frac{\partial}{\partial x}A(x)\frac{\partial P(x,\omega)}{\partial x} + \underbrace{\nabla_\perp^2 P(\rho,\theta,\omega)}_{=0} = \frac{s^2}{c_0^2}P(\rho,\omega) \tag{5}$$

at every axial location x.

When the pressure satisfies Laplace's equation, the velocity stream-function contours define velocity flux "tubes," perpendicular to the iso-pressure contours (Rayleigh, 1896, Vol. II, p. 4). If we treat the flow in each velocity flux-tube as independent, we may think of the volume velocity as constant within any tube. For example, when there is a bend in the canal, the path length on the outside of the bend is longer than on the inside, thus has a greater delay. This argument seems to be similar to that of (Weibel, 1955).

At any point the force density vector $\mathbf{F}(r,\theta,z,\omega)$ may be computed from the pressure at that point, as

$$\mathbf{F}(r,\theta,z,\omega) = -\nabla P(r,\theta,z,\omega). \tag{6}$$

For frequencies below the canal cutoff frequency of 27 [kHz], the radial and angular components of the force are zero, leaving only a plane wave.[3]

The net result is that any radial variation in the pressure creates radial wave motion, that travels so fast, relative to the radial dimension of the canal, that it settles to a constant within a few reflections. For the human ear canal $2r_0 = 7.5$ [mm]. Thus this travel time is $\tau = 0.75/34300 \approx 22$ [μs]. This

[3] Since there are no sources in the medium, from Gauss's Law, $\nabla \cdot \mathbf{F} = \nabla^2 P = 0$. The only force on the medium is the inertial force, which based on the QS approximation, may be ignored.

is a "microscopic" description (i.e., at the [μs] scale) of how the non planer part of the wave (i.e., the higher order modes) goes to zero as the wave propagates down the canal.

The main point here is that due to an area change, distributed reflections introduce a frequency dependent axial delay. Experimentally this has been shown to be the case, and may be quantified by factoring the ear canal complex reflectance $\Gamma_m(f)$ into an allpass and minimum-phase factors (Robinson et al., 2013). The allpass factor defines the frequency dependent delay. In the following sections it shall be be shown that this frequency dependent delay is captured by the middle ear plane-wave model of Parent and Allen (2007, 2010).

Returning to our case of the complex modes of vibration of the TM, the only mode that can propagate from the TM to the tragus is the zeroth order plane wave (Morse, 1948).

To clarify the role of canal area change, two relevant examples from the literature are presented: i) a tube with a small constriction (Karal, 1953) and ii) lossy wave propagation in acoustic wave-guides (Mason, 1928).

1.1 Cavity with a constriction

We begin with the most simple case of an area change: a closed cavity with a constriction (Karal, 1953).

Karal correction: Consider the geometry of a cavity composed of a cascade of thee tubes having lengths l_1, l_2, l_3, a total length of $L = l_1 + l_2 + l_3$, and diameters d_1, d_2, d_3. The middle tube forms a constriction, meaning it is small relative to the other dimensions ($d_2 \approx l_2 = 2$ [mm] $\ll L$). Plane wave propagation is assumed for each of the three wave-guide segments.

Further suppose that a plane wave is propagating from the left into the constriction. To model the wave on either side of the constriction we expand the pressure in a spatial Fourier (i.e., eigenfunction) series (Karal, 1953). As the sound enters and leaves the constriction region, the wavefront adjusts to the constriction at the speed of sound. Assuming the cavity diameter is much less than the wavelength ($d < \lambda_c/2\pi = c_0/\omega_c$), the radial component is almost instantly reflected back by the cavity walls. Many such reflections occur as the wave propagates. Due to the rapid reflections, the radial and angular components of the pressure wave obey Laplace's Equation, as dictated by Eq. 5.

Karal's analysis of the spreading mass: Following a full modal analysis of a step junction, Karal (1953) defined an equivalent circuit for the wave at the junction by proving that the mode conversion is equivalent to a series mass M_K given by

$$M_K = \frac{4\rho}{3\pi^2 a}\left((1-\alpha) + (1-\alpha)^2\right). \tag{7}$$

The relationship between the size of the jump in radius is characterized by the ratio of the two radii, $\alpha = b/a$, where $b < a$, namely where the middle section is smaller than the first section.[4] The ratio α is always taken to be between zero and 1. In electrical terms, a mass is mathematically equivalent to an inductor.

Experimental results of a constriction: Figure 1 shows experimental data (short dash) for the group delay of a cascade of Plexiglas cylindrical tubes: Tube 1 ($l_1 = 6.3$, $d_1 = 7.4$ [mm]), representing a short piece of ear canal, is connected to a sealed cavity ($l_3 = 8.5$, $d_3 = 19.1$ [mm]), via a 2 [mm] constriction ($l_2 = 2.4$, $d_2 = 2.15$ [mm]). The other two model curves are based on a cascade of three

[4]This analysis works just as well for the case of an expansive section. In this case $\alpha = a/b$.

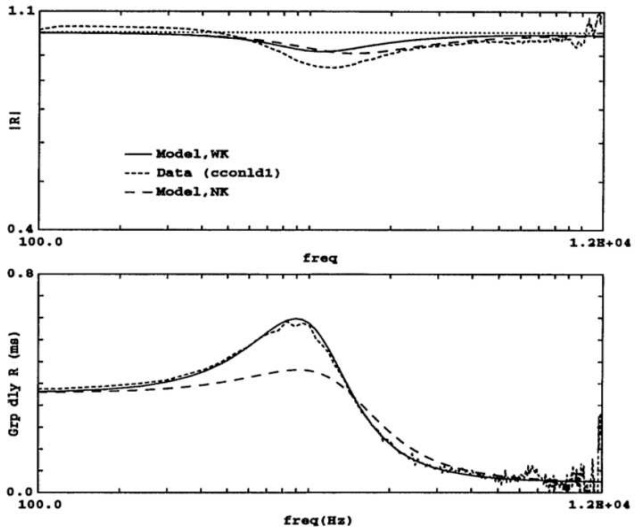

Figure 1: *Figure 5.7 from Puria (1991, p. 161), showing the reflectance magnitude (upper panel) and group delay (lower panel) for experimentally measured (short-dash) and modeled (solid-line) group delay, for a cascade of two transmission lines, coupled by a 2 [mm] constriction. When the Karal spreading mass is included at each junction, the group delay of the experimental data and model closely match. When the spreading mass is removed (Model, NK), the group delay at 0.9 kHz drops from 0.64 to 0.464 [ms], a 27% drop. It is this increase in delay at 0.9 kHz that caused the first impedance zero to shift from 2.2 to 0.9 [kHz] (a factor of 2.44), in agreement with the change in the phase at that frequency. At frequencies above 4 [kHz], the delay approaches 40 μs, corresponding to a round trip delay in the first tube ($\tau = 2L/c_0 = 2 * 0.0063/343 = 38[\mu s]$). The first impedance pole shifts down from 4 to 3.1 [kHz] (not shown) due to the large net phase change at that frequency.*

transmission lines, coupled with (WK: solid line) and without (NK: long dash) two series spreading masses, placed on either side of the constriction, as outlined by (Karal, 1953, Fig. 4). Adding the spreading mass (WK) decreases the first impedance zero (not shown) from 1.2 to less than 1 [kHz], and the first impedance pole from 4 to 3.1 [kHz]. This shift is explained by the change in the phase at the pole and zero frequencies. Of special interest is the large peak in the group delay at 0.9 [kHz] of ≈ 0.64 [ms] with the addition of the spreading mass [WK], in excellent agreement with the measured data (short dashed line). Without the added mass terms [NK] the group delay is $\approx$0.464 [ms] at 0.9 [kHz]. The magnitude of the reflectance is slightly less than one at this frequency, indicating that there is a small increased loss at the constriction, due to viscous and thermal losses.

Thus varying the cross-sectional area greatly impacts the group delay, in a frequency dependent manner.

1.2 Example 2: Lossy wave-guide propagation

The second example is the case of lossy wave propagation, where the losses are due to viscous and thermal damping. This problem of viscous loss in sound transmission was first worked out by Helmholtz (1863) and then extended by Kirchhoff (1868) to include thermal damping (Rayleigh, 1896, Vol. II, p. 319). These losses are explained by a modified complex propagation function $\kappa(s)$ (Eq. 1). Following a review of these theories, Crandall (1926, Appendix A) noted that the "Helmholtz-Kirchhoff" theory had never been experimentally verified. Acting on this suggestion, Mason (1928) set out to experimentally verify the theory.

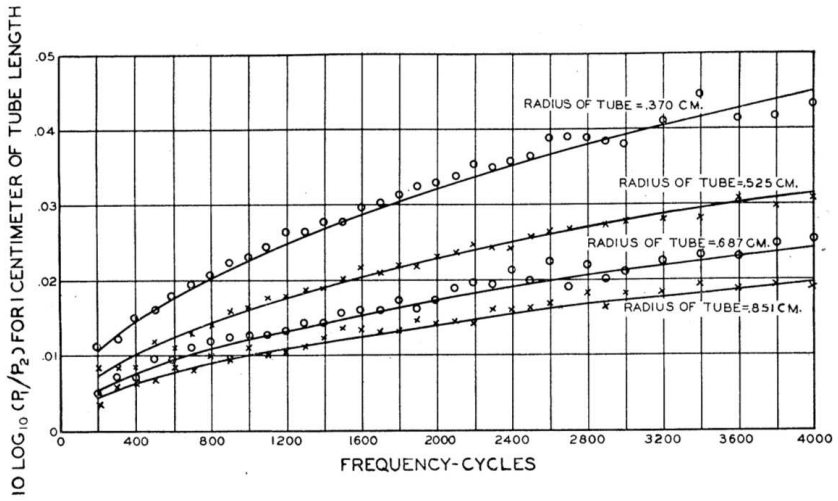

Figure 2: *This figure, taken from Mason (1928), compares the Helmholtz-Kirchhoff theory for $|\kappa(f)|$ to Mason's 1928 experimental results measurement of the loss. The ratio of two powers (P_1 and P_2) are plotted (see Mason's discussion immediately below Fig. 4), and as indicated in the label: "$10 \log_{10} P_1/P_2$ for 1 [cm] of tube length." This is a plot of the transmission power ratio in [dB/cm].*

1.2.1 Mason's Specification of the propagation function

Mason's results are reproduced here in Fig. 2 as the solid lines for tubes of fixed radius between 3.7–8.5 [mm], having a power reflectance given by

$$|\Gamma_L(f)|^2 = \left|e^{-\kappa(f)\,L}\right|^2 \tag{8}$$

[dB/cm].

The complex propagation function was given by Mason (1928, Eq. 2) as

$$\kappa(\omega) = \frac{P\gamma'\sqrt{\omega}}{2c_0 S\sqrt{2\rho}} + \frac{i\omega}{c_0}\left\{1 + \frac{P\gamma'}{2S\sqrt{2\omega\rho}}\right\}, \tag{9}$$

where S is the tube area and P is the *perimeter*. Here $\gamma' = \sqrt{\mu}\left[1 + \sqrt{5/2}\left(\gamma^{1/2} - \gamma^{-1/2}\right)\right]$ is a thermodynamic constant.

Mason specified physical constants for air to be $P_0 = 10^5$ [Pa] (atmospheric pressure), $\gamma = 1.4$ (ratio of specific heats), $\rho = 1.2$ [kgm/m^2] (density), $c_0 = \sqrt{P_0\gamma/\rho} = 341.56$ [m/s] (lossless velocity of sound), $\mu = 18.6 \times 10^{-5}$ [Pa-s] (viscosity),

Equation 9 and the measured data are compared in Fig. 2, reproduced from Mason's Fig. 4. Keefe (1984, Eq. 11) formulation for κ was also compared to Masons formula, and the agreement was again excellent.

With some algebra, Eq. 9 may be expressed in terms of s as[5]

$$\kappa(s) = \frac{s}{c_0} + \frac{\beta_0}{c_0}\sqrt{s} \tag{10}$$

where $\beta_0 = P\gamma'/2S\sqrt{\rho}$ is a constant. For the case of a cylindrical ear canal the radius is $R = 2S/P$, thus $\beta_0 = \gamma'/R\sqrt{\rho}$.

Note how the propagation function has a Helmholtz-Kirchhoff correction for both the real and imaginary parts. This means that both the speed of sound and the damping are dependent on frequency, proportional to $\beta_0\sqrt{s}/c_0$. Note also that the smaller the radius, the greater the damping.

[5]The real and imaginary parts of this expression, with $s = i\omega$, give Eq. 9.

In summary, the Helmholtz-Kirchhoff theory of viscous and thermal losses results in a frequency dependent speed of sound, having a frequency dependence proportional to $1/\sqrt{\omega}$ (Mason, 1928, Eq. 4). This corresponds to a 2% change in the sound velocity over the decade from 0.2-2 [kHz] (Mason, 1928, Fig. 5), in agreement with experiment.

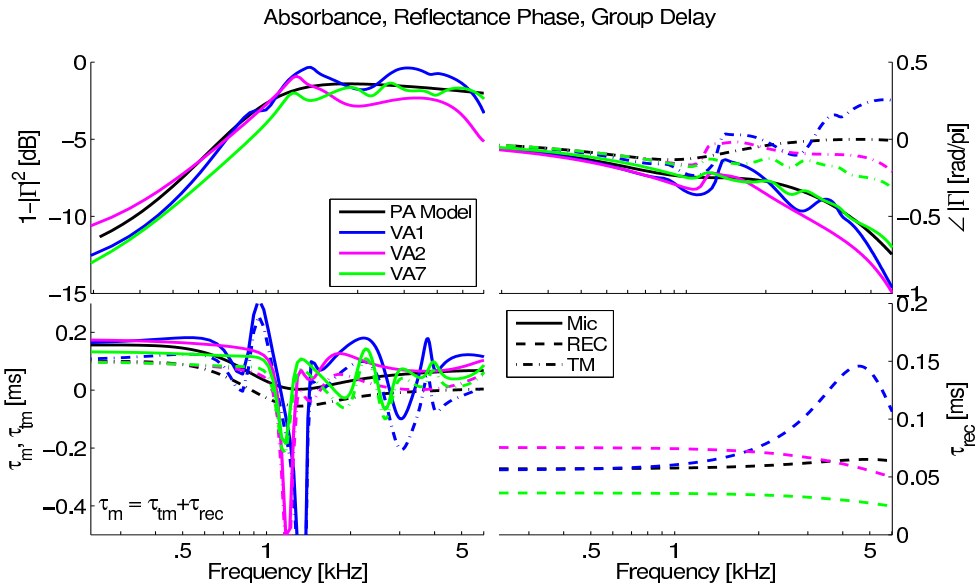

Figure 3: *This figure shows a direct comparison of reflectance measurements for three human ears (solid gray lines) (Voss and Allen, 1994) to the middle ear model of Parent and Allen (2010) (black solid line). In each panel the three solid gray curves are for VA subjects 1, 2 and 7 while the solid black line is for the PA-10 model. There are four panels: Upper-left:* Absorbance-level *(i.e., $|1-\Gamma(f)|^2$, in [dB]); Lower-left: Reflectance group delay measured at the microphone ($\tau_m(f)$) (solid lines), along with the minimum-phase TM group delay $\tau_{tm}(f)$ (dash-dot lines)), obtained by the reflectance factorization method (Robinson et al., 2013) (see the text for the details on this factorization); Upper-right: Phase of the complex reflectance ($\angle\Gamma(f)$) at the microphone (solid lines) and at the TM minimum-phase (dash-dot lines). Lower-right:* Residual ear canal *allpass factor group delay $\tau_{rec} = \tau_m - \tau_{tm}$, namely the difference between the solid and dashed lines of the lower-left panel. The group delay for subject VA1 (gray dashed line) with the large peak of 0.15 [ms] at 5 [kHz] is similar to the group delay of Fig. 1, suggesting that there is a constriction at the probe tip for this ear.*

2 Parent and Allen model

In the proceeding section we have show that a change in canal area introduces an allpass filtering effect such that the reflectance group delay becomes a function of frequency. Based on the Helmholtz-Kirchhoff formula, the lossy propagation function may be generalized to have a $\sqrt{s}$ dependence, as given by Eq. 10.

In the following we compare the Parent and Allen (2010) model (PA-10) with acoustic impedance data (Voss and Allen, 1994) from human ears and artificial ear couplers. The method we use for this comparison is the *reflectance factorization method* (Robinson et al., 2013). This method uniquely decomposes the complex reflectance into allpass and minimum-phase factors

$$\Gamma_m = \Gamma_{rec}\Gamma_{tm}, \tag{11}$$

where Γ_m is the complex reflectance measured at the microphone, Γ_{rec} accounts for the delay between the microphone and the TM (residual ear canal), while Γ_{tm} is the minimum-phase reflectance looking into the TM. This decomposition takes advantage of the mathematical properties of the two factors, providing a precise mathematical separation of the two components (Robinson et al., 2013). The magnitude of the all pass factor is 1 ($|\Gamma_{rec}| = 1$). Thus the microphone power reflectance equals the TM factor ($|\Gamma_m(f)| = |\Gamma_{tm}(f)|$). This rigorously solves the problem that tympanometry fails to solve.

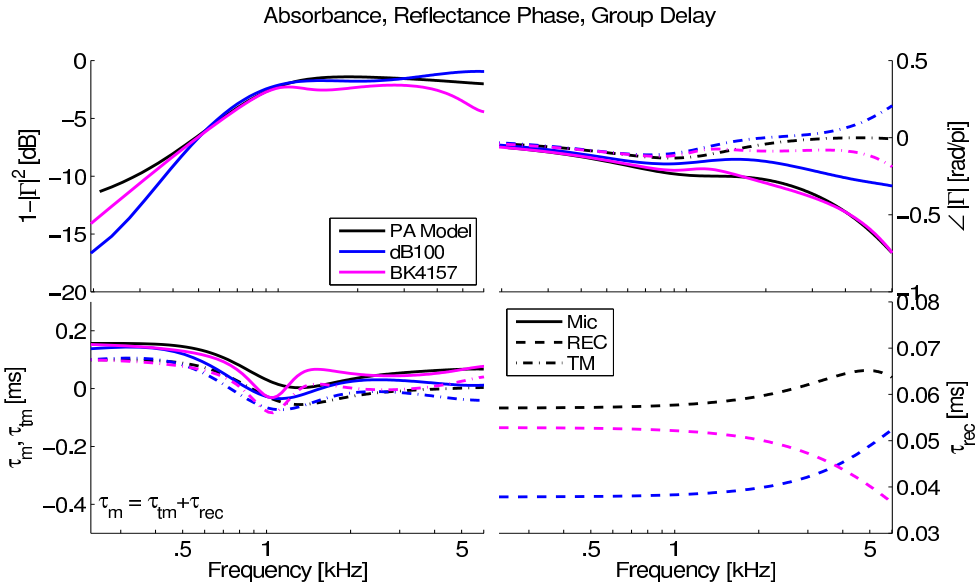

Figure 4: *This figure shows the reflectance for two commercially available middle ear couplers (BK-4157, DB-100) (Voss and Allen, 1994), in the same format as Fig. 3. As previously observed (Parent and Allen, 2010), the coupler data and the PA-10 model are very similar, with the model fit to the coupler data much closer than to the human ears. The model captures the frequency dependent allpass dependence wave propagation in the ear canal.*

The fundamental assumption of tympanometry is that when the canal is pressurized, the TM compliance is zero. This condition has been shown to be inaccurate (Rabinowitz, 1981). The factorization of the reflectance allows us to accurately compute the TM impedance, with the ear canal delay precisely removed, independent of any canal area changes. This solves a long standing problem in clinical acoustics, inaccurately addressed by the tympanometry methodology.

The residual canal factor (Γ_{rec}) characterizes the residual ear canal space (and TM delay) as an allpass response (phase only), while the TM factor characterizes the *minimum-phase* component of the TM, independent of the canal. Assuming the canal area is not constant, it is expected that this allpass factor will have a delay that depends on frequency. The question being addressed here is how the PA model results compare to the human data.

Reflectance/Absorbance plots: Figures 3, 4 compare the absorbance (i.e., $\mathcal{A}(f) = 1 - |\Gamma_m(f)|^2$, namely 1 minus the power reflectance), and the factored group delay (slope of the reflectance phase) for three normal human ears (Fig. 3) and two industry couplers (Fig. 4), to the Parent and Allen (2010) model. Details are provided in the figure captions. The general conclusion is that PA-10 fits the coupler data very well, but, like couplers, does not match the detailed variations in human data. The source of these small (i.e., 1 dB) fluctuations seem to be related to standing waves on the TM. The details of this interesting possibility must be postponed for now.

Reflectance Polar plots: Figure 5 show reflectance *polar plots* corresponding to the data of Figs. 3, 4. These are plots of the real vs imaginary parts of the complex reflectance $\Gamma(f)$, with frequency as a parameter. It follows that by precisely removing the residual canal delay, estimates of the TM impedance have a greatly reduced variance.

In the left most figure there are three colored curves (VA1,2,7), one black curve (PA model), and four (superimposed) Γ_{rec} plots (dashed lines). Since the reflectance goes to 1 at low frequencies, all the polar plots converge to 1 (all the curves meet at coordinates 0,1). As frequency increases, the phase advances and the reflectance magnitude decreases. Between 1 and 3 kHz, the reflectance magnitude forms loops in the polar plots. These loops are the same as the 1 [dB] oscillations across frequency

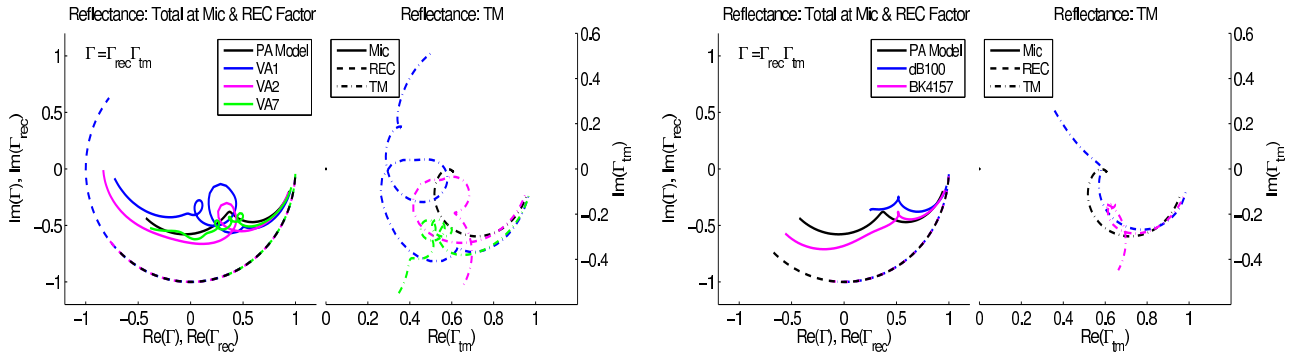

Figure 5: *These figures show* polar *diagrams for the Voss and Allen (1994) human data of Fig. 3 (left), and the artificial ear coupler data of Fig. 4 (right). Each polar plot displays the real part (x axis) vs. the imaginary part (y axis) of the complex reflectance, centered about the origin. Data of Fig. 3 (left-most panels): This shows (solid lines)* $\Gamma_m(f)$*, measured at the microphone, for the three human subjects, along with the PA-10 model and the corresponding four allpass factors* Γ_{rec} *(superimposed dashed lines). The second right-most panel shows the tm factor (*Γ_{tm}*) for the same three human ears and the Parent and Allen (2010) model. Data of Fig. 4 (right-most panels): This shows the artificial ear couplers (dB-100, BK-4157), in the same format as the human data on the right.*

in the absorbance. The second panel (from the left, (Fig. 3) is the minimum-phase reflectance factor of the TM, with the ear canal component removed. Note how the real part of this factor remains positive. The third panel (from the left) is the total reflectance of the couplers, as measured by the transducer microphone. The right-most panel is the coupler minimum-phase TM factor Γ_{tm} following the removal of the allpass factor $\Gamma_{rec}(f)$.

When the reflectance forms a piece of a circle (black dashed curve on the left), with no cusp or loop, the magnitude of the reflectance is 1, and its phase is increasing with frequency, forming a circle. This is the signature of a rigid cavity.

The minimum phase polar plots present the complex reflectance in a novel way, that tells the story about each ear, in terms of both magnitude and phase. With some training one can learn to relate the absorbance and polar plots for a given ear, as they are closely related. For example, the couplers and the PA-10 model have no loops, just a slight cusp near 1 [kHz], whereas the human ears exhibit large loops which are related to the small oscillations in the magnitude as seen in the three human ears (VA1,2,7) of Fig. 3 (upper-left). Such oscillations are not present in the model or the couplers. There is strong evidence that the loops are related to standing waves on the TM, not present in the model and couplers.

3 Discussion

Two publications have recently appeared criticizing PA-10. The first (Serwy, 2014) makes several incorrect claims, discussed below. The second (Shera, 2014) followed with some of the same points, along with suggested modifications to Srewy's claims. The main problem with both of these articles is their formulation of the problem due to a misunderstanding of the PA-10 model equations. Both articles are concerned that PA-10 has failed to provide the basic equations of their model. To address this point, we provide these equations in Appendix A.

3.1 Comments on PA-10 by Serwy (2014) and Shera (2014)

The main claim of both articles is that PA-10 violates conservation of energy. However by direct calculation it is easily verified that the power reflectance $|\Gamma_m|$ is less than 1, in both directions. We contend that if the power reflectance is less than 1, conservation of energy is not violated. Furthermore the

model is stable (the solution does not become unstable), and accurately fits the experimental coupler data, both in magnitude and phase (Fig. 5).

Shera's claims: Shera's additional argument is his application of the "lumen method" to "text-book examples," which, he claims, proves that the method used by PA-10 violates conservation of energy. However Shera's "textbook" example is incorrect. Specifically, his solution to a the problem of a jump in area of a tube is incorrect because the solution requires a Karal spreading mass, which he ignores. We have experimentally verified the role of the Karal spreading mass, required when modeling a rapid change in area (i.e., Fig. 1).

Serwy's claims: The analysis by Serwy is incorrect as he has ignored the delay elements, near and on the TM, used by the PA-10 model. These variable delays are necessary to implement the frequency dependent delay, required to simulate the frequency dependent delay that results from the change in area with x (Figs. 3, 4).

Serwy further claimed that PA-10 violated reciprocity. It seems a bit unreasonable to criticize how PA-10 model violates reciprocity, given that PA-10 has discussed this violation in great detail. Serwy has failed to acknowledge this detailed discussion.

In summary, both of these papers have relied on an analysis that ignores the change in area of the ear canal, which requires the application of the Webster Horn (Eq. 4). They both quote the work of Bilbao (2004), which assumes a three-dimensional quasi-static model, which does not treat the required change in area with x.

As supported by Figs. 3,4, PA-10 gives an allpass canal response, as desired to match real data (e.g., the coupler data of Fig. 4).

Given the rather close fit of PA-10 in both magnitude and phase, and the observation of a variable group delay in the allpass component, it seems to this author that the model is working quite well, and that both sets of criticisms are unfounded, and their analysis methods flawed.

Modeling an ear canal having variable area, along with the ear-drum, with its complex vibration, requires a deep understanding of higher order mode propagation. It has been the goal of this report, to provide some of this insight.

4 Conclusions

Two exact classic solutions to acoustic wave propagation in an ear canal having a variable area $A(x)$, have been presented. The first case (Fig. 1) is a loss-less constriction, the second (Fig. 2) is the inclusion of viscous and thermal losses at the canal walls. In both cases the area is a function of frequency. Losses may be modeled by a thin *boundary layer* thickness that is frequency dependent. While this thickness is very small relative to the canal radius, it has a large effect. Besides introducing damping in the wave, losses modify the speed of sound so that it is frequency dependent (Mason, 1928). While this effect is only a few percent, it clearly enforces the point that an area change is equivalent to an allpass filter in the canal transfer function.

Thus in both examples, the effect of changing the area is to make the delay a function of frequency. Another way of saying this is that a variable canal area introduces an allpass filter effect.

We have also presented reflectance data for three human ears (Fig. 3), two artificial ear couplers (Fig. 4), and compared them to the Parent and Allen (2010) middle ear model. Each of these cases is analyzed using the reflectance factorization method. The factored reflectance precisely separates the canal from the TM, allowing one to directly model the TM impedance. The factored TM reflectance may then be converted back into the TM impedance, and modeled with a small number of parameters.

This allows one to accurately estimate the middle ear function in a systematic way, independent of the residual ear canal volume.

From the results presented here it is clear that the model is much closer to the coupler data in its response, both in magnitude and phase, than to the human ears. We believe that this difference is due to standing waves on the TM, which introduce the loops seen in Fig. 3.

The intent of PA-10 was to characterize the canal impedance and reflectance using a time-domain model, and thus to model the cochlear pressure. The intent was not to characterize the reverse transfer function. Today there is a need to characterize reverse transmission and understand the role of standing waves on the TM. Achieving these goals will require significant extensions to PA-10.

Notably the ear canal allpass group delay of the Parent and Allen (2010) model shows a frequency dependent delay, similar to real ears. Except around the TM, the model assumes a uniform canal area, so the effect is small, but not zero. Thus the model is successful in simulating an allpass delay.

A Summary of PA-10 equations

Wave variables:

Canal:

$$\begin{bmatrix} P_c \\ V_c \end{bmatrix} = \begin{bmatrix} r_c & r_c \\ 1 & -1 \end{bmatrix} \begin{bmatrix} V_c^+ \\ V_c^- \end{bmatrix}. \tag{A.1}$$

$$r_c = \frac{P_c^\pm}{V_c^\pm} = \frac{p_n^\pm}{v_n^\pm} \tag{A.2}$$

$$\text{Specific Stiffness} = \eta P_0 = \rho_0 c^2; \qquad \text{Specific mass} = \rho \tag{A.3}$$

$$r_c = \rho_0 c / A_c; \qquad c = \sqrt{\text{stiffness}/\text{mass}} = \sqrt{\frac{\eta P_0}{\rho}} \tag{A.4}$$

TM:

$$\begin{bmatrix} F_m \\ U_m \end{bmatrix} = \begin{bmatrix} r_m & r_m \\ 1 & -1 \end{bmatrix} \begin{bmatrix} U_m^+ \\ U_m^- \end{bmatrix}. \tag{A.5}$$

$$r_{tm} = \frac{F_{tm}^\pm}{U_{tm}^\pm} = \frac{f_n^\pm}{u_n^\pm} \tag{A.6}$$

$$\text{Specific Stiffness} = \rho_{tm} c_{tm}^2 \qquad \text{Specific mass} = \rho_{tm} \tag{A.7}$$

$$r_{tm} = \rho_{tm} c_{tm} / A'_m; \qquad c_{tm} = \sqrt{\text{stiffness}/\text{mass}} \tag{A.8}$$

Lumen sum relations:

$$V_c^+ \equiv \sum_{n=-N}^{N} v_n^+. \qquad V_c^- \equiv \sum_{n=-N}^{N} v_n^-, \tag{A.9}$$

$$U_m^+ \equiv \sum_n u_n^+, \qquad U_m^- \equiv \sum_n u_n^- \tag{A.10}$$

$$v_n^+ = \frac{A_n}{A_c} V_c^+. \qquad u_n^- = \frac{A_n}{A'_m} U_m^-. \tag{A.11}$$

The matrix representation of the Lumen IO is given by Eq. A.15. The air-TM Reflectance is

$$R_n = \frac{(\rho_{tm} c_{tm})_n - \rho_0 c}{(\rho_{tm} c_{tm})_n + \rho_0 c}, \tag{A.12}$$

the TR-BC condition:

$$R_{\pm(N+1)} = 0 \tag{A.13}$$

Finally the lumen condition is

$$A_c = \sum_{n=-N}^{N} A_n. \tag{A.14}$$

A.1 Analysis of PA-10 equations

Putting this all together

$$\begin{bmatrix} u_n^+ \\ v_n^- \end{bmatrix} = \begin{bmatrix} -R_n e^{-j\omega 2\tau_n^{TM}} & (1-R_n)e^{-j\omega(\tau_n^c+\tau_n^{TM})} \\ (1+R_n)e^{-j\omega(\tau_n^c+\tau_n^{TM})} & R_n e^{-j\omega 2\tau_n^c} \end{bmatrix} \begin{bmatrix} u_n^- \\ v_n^+ \end{bmatrix}. \tag{A.15}$$

On the left are the output wave variables while on the right are the input wave variables. Included are the canal τ_n^c and TM τ_n^{TM} delays, which depend on the acoustic path length, thus these delays depend on the lumen index n.

When $U_m^- = 0$, all the u_n^- inputs must be zero. Likewise when $V_c^+ = 0$, all the $v_n^+ = 0$. These represent useful constraints on the canal and cochlear (i.e., stapes) boundary conditions.

Referring back to the model figure of Parent and Allen (2010), if one assumes a zero manubrium velocity $U_m^- = 0$ (no input from the cochlea), the canal v_n^- and TM u_n^+ partial volume velocities are given by the weighted sum of delayed forward partial canal volume velocities v_n^+, weighted by the delayed TM lumen reflection coefficients

$$\begin{bmatrix} u_n^+ \\ v_n^- \end{bmatrix}_{U_m^-=0} = e^{-j\omega\tau_n^c} \begin{bmatrix} (1-R_n)e^{-j\omega\tau_n^{TM}} \\ R_n e^{-j\omega\tau_n^c} \end{bmatrix} v_n^+.$$

It follows that when the manubrium velocity $U_m^- = 0$ ($u_n^- = 0$), the canal reflection coefficient is

$$\Gamma_c(s)|_{U_m^-=0} \equiv \left.\frac{V_c^-}{V_c^+}\right|_{U_m^-=0} = \frac{1}{A_c}\sum_n e^{-j2\omega\tau_n^c} A_n R_n \le \sum_n \frac{A_n}{A_c}|R_n| \le 1,$$

thus the model is passive and stable, as numerically demonstrated by PA-10. An identical calculation at the manubrium for $\Gamma_m = U_m^+/U_m^-|_{V_c^+=0}$ shows the model is stable in the reverse direction. When the cochlea is drained, $\Gamma_m = -1$, and the system again must again be stable, since in this case the canal reflectance is the product of the three transfer functions U_m^+/V_c^+, U_m^-/U_m^+ and V_c^-/U_m^-, namely $-V_c^-/V_c^+$.

Similarly when $V_c^+ = 0$ (no input from the canal), the volume velocity is given by the delayed weighted sum of forward partial volume velocities, weighted by the TM lumen reflection coefficients. In vector form this is

$$\begin{bmatrix} u_n^+ \\ v_n^- \end{bmatrix}_{V_c^+=0} = e^{-j\omega\tau_n^{TM}} \begin{bmatrix} -R_n e^{-j\omega\tau_n^{TM}} \\ (1+R_n)e^{-j\omega\tau_n^c} \end{bmatrix} u_n^-.$$

B Webster Horn Equation

To find Eq. 4 we start from the basic equations of acoustics (Pierce, 1981, page 15)

$$\frac{d}{dx}\begin{bmatrix} \mathcal{P}(x,\omega) \\ \mathcal{V}(x,\omega) \end{bmatrix} = -\begin{bmatrix} 0 & \mathscr{Z}(s,x) \\ \mathscr{Y}(s,x) & 0 \end{bmatrix}\begin{bmatrix} \mathcal{P}(x,\omega) \\ \mathcal{V}(x,\omega) \end{bmatrix}. \tag{B.1}$$

The Fourier-transform pair of the average pressure and volume velocity are denoted as $p(x,t) \leftrightarrow \mathcal{P}(x,\omega)$ and $\nu(x,t) \leftrightarrow \mathcal{V}(x,s)$, respectively. Here we use the complex *Laplace frequency* $s = \sigma + j\omega$ when referring to the *per-unit-length impedance*

$$\mathscr{Z}(s,x) \equiv s\frac{\rho_0}{A(x)} = sM(x) \tag{B.2}$$

and *per-unit-length admittance*

$$\mathscr{Y}(s,x) \equiv s\frac{A(x)}{\eta_0 P_0} = sC(x), \tag{B.3}$$

to clearly indicate that these functions must be *causal*, and except at their poles, *analytic* in s.[6] Here $M(x) = \rho_0/A(x)$ is the horn's *per-unit-length mass*, $C(x) = A(x)/\eta_0 P_0$ *per-unit-length compliance*, $\eta_0 = c_p/c_v \approx 1.4$ (air), $\kappa(s) \equiv \sqrt{\mathscr{Z}\mathscr{Y}} = s/c$ is the *propagation function*, $c = \sqrt{\eta_0 P_0/\rho_0}$ is the speed of sound and $r_0(x) = \sqrt{\mathscr{Z}/\mathscr{Y}} = \sqrt{\rho_0\eta_0 P_0}/A(x) = \rho_0 c/A(x)$ is denoted the *surge resistance*.

To show that Eq. B.1 is equivalent to Eq. 4, take the partial derivative with respect to x (the x subscript represents the partial wrt x) of the Newton pressure equation, giving $\mathcal{P}_{xx} + \mathscr{Z}_x\mathcal{V} + \mathscr{Z}(s)\mathcal{V}_x = 0$. Next use the Newton and Hooke equations once again, to remove the velocity, giving $\mathcal{P}_{xx} - (\mathscr{Z}_x/\mathscr{Z})\,\mathcal{P}_x = \frac{s^2}{c^2}\mathcal{P}$.

To obtain Eq. 4 it is necessary to use *integration by parts*. To do this one must find the unique "integration factor" $\sigma(x)$:

$$\frac{1}{\sigma}\frac{\partial}{\partial_x}(\sigma\mathcal{P}_x) \equiv \mathcal{P}_{xx} + \partial_x \ln\sigma(x)\ \mathcal{P}_x(x) \tag{B.4}$$

By a direct comparison of the above to Eq. 5, we see that $\sigma_x/\sigma \equiv -\mathscr{Z}_x/\mathscr{Z}$. Thus $\partial_x \ln(\sigma)/ \equiv -\partial_x \ln(\mathscr{Z}) = \partial_x \ln(A)$, or

$$\sigma(x) \equiv A(x). \tag{B.5}$$

Following the integration step we may put Eq. B.5 into Eq. B.4 and obtain the Webster Horn equation Eq. 4 (Morse, 1948, p. 269).

Thus we see that for the Webster Horn equation the *physical meaning of the integration factor is simply the area function.* Physically this makes sense. It explains, for example, why the integration factor in the Sturm-Liouville theory must be strictly positive. While it seems likely that Morse (1948) must have been aware of this connection, to our knowledge, he did not explicitly state so in writing.

B.1 Primitive solutions $p^{\pm}(x,t)$

For each choice of area function used in Eq. B.1 there are two causal *primitive solutions* of the homogeneous (i.e., undriven) equation, identified as an *outbound* (right-traveling) and *inbound* (left-traveling) wave, denoted as the Laplace transform pair $p^{\pm}(x,t) \leftrightarrow \mathcal{P}^{\pm}(x,s)$.

Propagation function $\kappa(s)$ The primitive solutions of the horn equation always depend on a complex wave *propagation function* $\kappa(s)$, defined as the square root of the *product* of $\mathscr{Z}$ and $\mathscr{Y}$:

$$\kappa(s) \equiv \sqrt{\mathscr{Z}(s,x)\mathscr{Y}(s,x)} = \sqrt{\frac{s\rho_0}{A(x)} \times \frac{sA(x)}{\eta_0 P_0}} = \frac{s}{c}, \tag{B.6}$$

where the speed of sound is given by $c = \sqrt{\eta_0 P_0/\rho_0}$. Note how the area $A(x)$ cancels in this expression, making the speed of sound constant. While horns are, in general, dispersive, the wave-front speed is always constant.

In the case of the loss-less air-coupled horn, $\kappa(s)$ is independent of the range x. For the case of viscous and thermal losses, Eq. 10 may be used.

Examples: For the solution in a uniform pipe, the two primitive solutions are plane waves

$$\delta(t \mp x/c) \leftrightarrow \mathcal{P}^{\pm}(x,\kappa) = e^{\mp\kappa(s)x}.$$

These two directed wave solutions are functions of Laplace frequency s, since they must be causal. They may be viewed as the causal impulse response of a semi-infinite section of Eq. 4, driven at the input by an impulse at $t = 0$. The primitive solutions are normalized to a unit input.

[6] A function $F(s)$ is said to be *complex analytic* in s at point a if it may be represented by a Taylor series in $s - a$.

For the spherical geometry the outbound wave is $e^{-\kappa r}/r$. It contains a reflected component due the change in the area of the wave front, which gives rise to a reactive mass-component in the radiation impedance.

The exponential horn is of special interest because the radiation impedance is purely reactive below the horn's cutoff frequency.

B.1.1 Exponential Horn

Assuming that area $A(x) = A_0 e^{2mx}$, Eq.4 simplifies to

$$\mathcal{P}_{xx} + 2m\,\mathcal{P}_x = \kappa^2 \mathcal{P}(x,\omega). \tag{B.7}$$

Since the coefficient of $\mathcal{P}_x$ is a constant, resulting in an ordinary constant coefficient differential equation, having a closed form solution (Olson, 1947; Salmon, 1946a,b; Morse, 1948; Beranek, 1954; Leach, 1996). By the substitution $\mathcal{P}(x,\omega) = Ae^{\lambda x}$, one may solve for the *characteristic roots* ($\lambda_\pm(s) = m \pm \sqrt{m^2+\kappa^2}$) resulting in solutions

$$\mathcal{P}^{\pm}(x) = e^{\lambda_\mp} = e^{-mx} e^{\mp\sqrt{m^2+\kappa^2}\,x} = e^{-mx} e^{\mp j\sqrt{\omega^2-\omega_c^2}\,x/c}, \tag{B.8}$$

thus providing the horn's forward (+) and backward (-) solution for the pressure. Below cutoff the reflection coefficient magnitude is unity (no energy can radiate from an open horn. This is easily shown by computing the radiation admittance and observing that its real part is zero below the cutoff frequency.

C General solution of the Webster Horn Equation

An arbitrary area function cannot be solved in close form. Numerical methods and analytic power series are two general methods of attach. However their are approximate methods that work under some quite general conditions. The most important of these is called the WKB method. It is an approximate solution that assumes a slowly varying area, resulting in small reflections.

The WKB approximation This method is widely used in physics, for example in quantum mechanics. Given the equation

$$\frac{d^2}{dx^2}\Phi(x,s) = F(x)\,\Phi(x,s)$$

the effective *wave number* is

$$F(x) = \frac{2m}{\hbar^2}\left[V(x) - E\right]$$

and the WKB approximation gives the solution[7]

$$\Phi(x,s) = C\frac{e^{-i\int\sqrt{F(x)}dx}}{\sqrt[4]{F(x)}}$$

where C is a constant which is to be determined by the initial conditions.

This method consists of integrating the phase delay of the square-root wave number, as a function of the range variable. Picking the correct branch of the square root is essential in the application of this solution method. It should be obvious that the sign of F is critical to the solution, because the

[7] http://en.wikipedia.org/wiki/WKB_approximation

square root of a negative number is complex. Also essential is the unwrapping of the phase in the exponent under the integral of the square root of the effective wave number. One may conclude that the complex-analytic properties of the wave number are essential to the solution (the wave number is not a single valued function of x and s). In fact without an understanding of a branch cut, the WKB solution makes no sense. The WKB solution massively fails when $|\Gamma_L| \rightarrow 1$. It is interesting to consider this case for the exponential horn, since we have the exact solution for this case.

To study the general case we decompose the primitive solutions into forward and backward (i.e, D'Alembert) waves.[8] Denote P^+ and P^- as the forward and backward waves. Then

$$\left[\begin{array}{c} P \\ U \end{array} \right] = \left[\begin{array}{cc} z_0 & z_0 \\ 1 & -1 \end{array} \right] \left[\begin{array}{c} U^+ \\ U^- \end{array} \right] = \left[\begin{array}{cc} 1 & 1 \\ y_0 & -y_0 \end{array} \right] \left[\begin{array}{c} P^+ \\ P^- \end{array} \right].$$

Substituting this into Eq. B.1 we may write the horn equation in terms of forward and backward waves (Neely and Allen, 2009)

$$\frac{d}{dx} \left[\begin{array}{c} P^+ \\ P^- \end{array} \right] = \left[\begin{array}{cc} -\kappa - \epsilon & \epsilon \\ \epsilon & \kappa - \epsilon \end{array} \right] \left[\begin{array}{c} P^+ \\ P^- \end{array} \right]. \tag{C.1}$$

where $\epsilon(x) = \frac{1}{2}\frac{d}{dx} \ln A(x)$ and $\kappa = \sqrt{ZY} = s/c$. The characteristic polynomial of this system is

$$\Delta(\lambda) = \det \left[\begin{array}{cc} -\kappa - \epsilon - \lambda & \epsilon \\ \epsilon & \kappa - \epsilon - \lambda \end{array} \right] = 0 \tag{C.2}$$

having complex eigenvalues $\lambda_\pm = -\epsilon \pm \sqrt{\epsilon^2 + \kappa^2}$. Thus the decay is described by $e^{-\epsilon}$ and the propagation as $e^{\pm\sqrt{\epsilon^2+\kappa^2}}$.

The WKB solution may be obtained form Eq. C.1 by assuming that $|\kappa(x,s) + \epsilon(x)| >> |\epsilon(x)|$, that is, by ignoring P^-

$$\frac{dP^+}{dx} = -\left[\kappa(x,s) + \epsilon(x)\right] P^+. \tag{C.3}$$

The above may be directly integrated:

$$P^+(x,s) \approx P^+(0,s) e^{-\int_0^x [\kappa(x,s)+\epsilon(x)]dx}. \tag{C.4}$$

For the WHEN, κ is independent of x, yet the solution still dependents on x due to $\epsilon(x)$.

[8] This is basically an eigen-value transformation.

References

Allen, J. B. (1986). Measurement of eardrum acoustic impedance. In Allen, J. B., Hall, J. L., Hubbard, A., Neely, S. T., and Tubis, A., editors, *Peripheral Auditory Mechanisms*, pages 44–51, New York. Springer Verlag.

Beranek, L. L. (1954). *Acoustics*. McGraw–Hill Book Company, Inc., 451 pages, New York.

Bilbao, S. (2004). *Wave and scattering methods for numerical simulation*. Wiley, 398 pages, London.

Campbell, G. (1922). Physical theory of the electric wave filter. *Bell System Tech. Jol.*, 1(2):1–32.

Crandall, I. B. (1926). *Theory of Vibrating Systems and Sound*. D. Van Nostrand Company, Inc., 272 pages, New York. Book contains extensive Bibliographic information about applied acoustics and speech and hearing. Crandall was the first to analyze speech sounds in a quantitative way.

Farmer-Fedor, B. and Rabbitt, R. (2002). Acoustic intensity, impedance and reflection coefficient in the human ear canal. *The Journal of the Acoustical Society of America*, 112:600–620.

Hamming, R. W. (1977). *Digital Filters*. Prentice-Hal, Inc., 200 pages, Englewood Cliffs, NJ.

Helmholtz, H. L. F. (1863). *On the sensations of tone*. Dover (1954), 300 pages, New York.

Hunt, F. V. (1982). *Electroacoustics, The analysis of transduction, and its historical background*. The Acoustical Society of America, 260 pages, Woodbury, NY 11797.

Karal, F. C. (1953). The analogous acoustical impedance for discontinuities and constrictions of circular cross section. *J. Acoust. Soc. Am.*, 25(2):327–334.

Keefe, D. H. (1984). Acoustical wave propagation in cylindrical ducts: Transmission line parameter approximations for isothermal and nonisothermal boundary conditions. *J. Acoust. Soc. Am.*, 75:1386–1391.

Leach, W. (1996). A 2-port analogous circuit and SPICE model for Salmon's family of acoustic horns. *J. Acoust. Soc. Am.*, 99(3):1459–1464.

Lynch, J. T., Nedzelnitsky, V., and Peake, W. T. (1982). Input impedance of the cochlea in cat. *J. Acoust. Soc. Am.*, 72:108–130.

Mason, W. (1928). The propagation characteristics of sound tubes and acoustic filters. *Phy. Rev.*, 31:283–295.

Moller, A. R. (1960). Improved technique for detailed measurements of the middle ear impedance. *J. Acoust. Soc. Am.*, 32(2):250–257.

Morse, P. M. (1948). *Vibration and sound*. McGraw Hill, 468 pages, NYC, NY.

Neely, S. and Allen, J. B. (2009). Retrograde waves in the cochlea. In Cooper, N. P. and Kemp, D. T., editors, *Proceedings of the 10th Mechanics of Hearing Workshop*, pages 62–67. World Scientific Publishing Co., Singapore. In Press.

Olson, H. F. (1947). *Elements of Acoustical Engineering (2^n Edition)*. D. Van Nostrand Company, 539 pages.

Parent, P. and Allen, J. B. (2007). Wave model of the cat tympanic membrane. *J. Acoust. Soc. Am.*, 122(2):918–931.

Parent, P. and Allen, J. B. (2010). Wave model of the human tympanic membrane. *Hearing Research*, 263:152–167.

Pierce, A. D. (1981). *Acoustics: An Introduction to its Physical Principles and Applications*. McGraw-Hill, 678 pages, New York.

Puria, S. (1991). *A theory of cochlear input impedance and middle ear parameter estimation*. PhD in Electrical Engineering, City University of New York, 211 pages, UMI, 300 N. Zeeb Rd, Ann Arbor MI, 48106; Order Number 9119669.

Puria, S. and Allen, J. B. (1998). Measurements and model of the cat middle ear: Evidence for tympanic membrane acoustic delay. *J. Acoust. Soc. Am.*, 104(6):3463–3481.

Rabinowitz, W. M. (1981). Measurement of the acoustic input immittance of the human ear. *J. Acoust. Soc. Am.*, 70:1025–1035.

Rayleigh, J. W. (1896). *Theory of Sound, Vol. I 480 pages, Vol. II 504 pages*. Dover, New York.

Robinson, S., Nguyen, C., and Allen, J. (2013). Characterizing the ear canal acoustic impedance and reflectance by pole-zero fitting. *Hearing Research*, 301:168–182.

Salmon, V. (1946a). Generalized plane wave horn theory. *J. Acoust. Soc. Am.*, 17(3):199–211.

Salmon, V. (1946b). A new family of horns. *J. Acoust. Soc. Am.*, 17(3):212–218.

Serwy, R. (2014). Comment on "Wave model of the cat tympanic membrane" (L). *J. Acoust. Soc. Am.*, 135(5):2493–6.

Shera, C. (2014). On the method of lumens. *J. Acoust. Soc. Am.*, 136(6):3126–3131.

Voss, S. E. and Allen, J. B. (1994). Measurement of acoustic impedance and reflectance in the human ear canal. *J. Acoust. Soc. Am.*, 95(1):372–384.

Webster, A. G. (1919). Acoustical impedance, and the theory of horns and of the phonograph. *Proc. Nat. Acad. Sci.*, 5:275–282.

Wegel, R. L. and Lane, C. (1924). The auditory masking of one pure tone by another and its probable relation to the dynamics of the inner ear. *Physical Review*, 23:266–285.

Weibel, E. (1955). On Webster's horn equation. *J. Acoust. Soc. Am.*, 27(4):726–727.

Zwislocki, J. (1950). Theory of the acoustical action of the cochlea. *J. Acoust. Soc. Am.*, 22:779–784.